Physica C 469 (2009) 2044–2051

Contents lists available at ScienceDirect

Physica C

journal homepage: www.elsevier.com/locate/physc

Magnetic field orientation dependence of flux pinning in (Gd,Y)$Ba_2Cu_3O_{7-x}$ coated conductor with tilted lattice and nanostructures

Y. Zhang [a,*], E.D. Specht [a], C. Cantoni [a], D.K. Christen [a], J.R. Thompson [a,b], J.W. Sinclair [b], A. Goyal [a], Y.L. Zuev [a], T. Aytug [a], M.P. Paranthaman [a], Y. Chen [c], V. Selvamanickam [c]

[a] Oak Ridge National Laboratory, Oak Ridge, TN 37831, USA
[b] The University of Tennessee, Knoxville, TN 37996, USA
[c] SuperPower Inc., Schenectady, New York 12304, USA

ARTICLE INFO

Article history:
Accepted 20 August 2009
Available online 25 August 2009

PACS:
74.25.Qt
74.25.Sv
74.62.Dh
74.72.Bk

Keywords:
Flux pinning
Coated conductor
Critical current density
Anisotropy
Extended nanoparticle defects

ABSTRACT

The dependence of the critical current density (J_c) on the orientation of an applied magnetic field was studied for a prototype (Gd,Y)$Ba_2Cu_3O_{7-x}$ (GdYBCO) coated conductor fabricated by MOCVD on an IBAD-MgO template. Additional rare-earth cations (Y and Gd) and Zr were incorporated into the superconducting film to form $(Y,Gd)_2O_3$ and $BaZrO_3$ nanoparticles extended nearly parallel to the *a–b* planes and to the *c*-axis, respectively, to enhance the flux pinning. In-field measurement of J_c was carried out with electrical current flowing either along or perpendicular to the longitudinal axis of the tape, while a maximum Lorentz force configuration was always maintained. Details in the angular dependence of J_c were related to the unique structure of the film, specifically the tilt in the GdYBCO lattice and the tilts in the extended $(Y,Gd)_2O_3$ and BaZrO3 nanoparticles. XRD and TEM were used to study the structure of the coated conductor. The effect of the misalignment between the external field **H** and the internal field **B** on the angular dependence of J_c is discussed.

© 2009 Elsevier B.V. All rights reserved.

1. Introduction

The development of $YBa_2Cu_3O_{7-x}$ (YBCO)-based coated conductors aims at many applications such as motors, generators and transformers, all involving the presence of magnetic fields from intermediate to high strengths. In-field performance of the superconducting tapes, dependent on not only the strength but also the orientation of the applied magnetic field, is crucial for these applications. The in-field performance, specifically the critical current density (J_c), can be enhanced by introducing various structural and morphological defects with appropriate size and distribution that effectively pin the magnetic vortices [1]. In the last several years, extensive efforts in engineering and optimizing the defects at a nanometer scale using various techniques have made great progress, leading to significant advance in the coated conductor technology.

The relationship between critical current densities and the orientation of an applied magnetic field has been a topic of enormous theoretical and technological importance for high-T_c oxide superconductors. Electronic and structural anisotropy is recognized as a major source, accounting for the phenomenon that the J_c value varies with applied field orientation. Indeed, the layered lattice itself can provide strong vortex pinning, arising from the intrinsic periodic modulation of the order parameter from inter- to intra-CuO_2 layers [2–4]. For a typical coated conductor where an epitaxial film is deposited on a biaxially textured template, the *a–b* plane of the lattice is normally parallel to the film surface or the film/substrate interface. The magnetic field angular dependence of J_c usually features a maximum when the applied field is parallel to the tape surface. This J_c maximum, denoted as the *a–b* peak, which is produced by a combined effect of the electronic mass anisotropy, intrinsic pinning, and layered defects has been reported for YBCO films fabricated by various techniques such as PLD (pulsed laser deposition) [5,6], sputtering [7], MOCVD (metal organic chemical vapor deposition) [8], MOD (metal organic deposition) [9] and electron-beam evaporation [10]. It is worth to note that layered intergrowths typically contribute significantly to the observed *a–b* peak, and that for any practical HTS coatings, there are always various types of structural defects acting as flux pinning centers. A finite $J_c(\theta)$, including a J_c maximum, is sustained by the combined effects from the layered lattice and from any contributing struc-

* Corresponding author. Tel.: +1 8655746264; fax: +1 8655746263.
E-mail address: zhangyf@ornl.gov (Y. Zhang).

0921-4534/$ - see front matter © 2009 Elsevier B.V. All rights reserved.
doi:10.1016/j.physc.2009.08.007

tural defects. In general, $J_c = F_p/B$, where F_p is the macroscopic volume pinning force exerted on the flux lines by all possible pinning centers. The angular dependence of J_c is just a reflection of how these pinning effects vary with the external magnetic field orientation.

In an angular dependence measurement system, the orientation of the applied magnetic field is usually referenced to the film surface or normal. Under certain circumstances, the crystal lattice of the superconductor layer may tilt by a small angle from the film/substrate interface, so that the *a–b* planes are no longer parallel to the film surface. Consequently, the *a–b* peak may be found to shift from its "usual" reference position. The crystal lattice may tilt when a film is deposited on a vicinal single crystal substrate surface [11–13], on an IBAD (ion beam assisted deposition) template [14], or on an ISD (inclined surface deposition) template [15,16]. The exact mechanism responsible for this out-of-plane tilt is beyond the scope of this paper, but its effect on in-field J_c anisotropy is to be considered.

When analyzing angular dependent J_c data, it is important to note that there may be a misalignment between the orientations of the internal field (**B**) and the external field (**H**). It is the orientation of **B** rather than **H** that determines when a flux pinning effect is maximized. For example, strictly, the *a–b* peak should occur where the internal field (**B**) is parallel to the *a–b* plane. If there are other J_c peaks, they should appear where **B** is parallel to the responsible extended pinning centers, e.g., columnar nanoparticles, which have an angularly preferential distribution.

The orientation of the internal field **B** is determined by several combined or competing factors. Firstly, vortex lines have a strong tendency to minimize the total energy by shortening their lengths. For a thin film sample, the geometric demagnetizing effect tends to align the vortex lines parallel to the normal to the surface. Secondly, vortex lines prefer to be parallel to the magnetizing field in order to minimize the magnetic energy. Thirdly, vortex lines in an anisotropic superconductor such as YBCO tend to tilt toward the direction of the *a–b* plane to reduce their line energy per unit length. Lastly, since pinning by correlated disorder always reduces the system energy, vortex lines incline to align themselves parallel to extended defects that act as effective pinning centers, such as those columnar nanoparticles formed during the process of film fabrication. Depending on the strength and the relative orientation of the applied field, one factor can be dominant while another or others may be small. It is the combined effect of all the above factors that determines the final orientation of **B** and that is why the internal field **B** often does not coincide with the external field **H**. As an angular dependence of J_c is most likely documented with respect to the orientation of the external applied field, this misalignment between **B** and **H** needs to be carefully considered when experimental results are interpreted and analyzed.

Structural defects play a central role in vortex pinning. Potential pinning defects include point defects such as vacancies and cation disorder, dislocations, twin boundaries, stacking faults, grain boundaries, and precipitates or inclusions of secondary phases. Insight into the nature of an effective flux pinning defect can be found within the $J_c \sim \theta$ relationship. For uncorrelated defects, which have a random distribution and an isotropic geometry, the pinning effect should depend on the effective field described by the supercarrier electronic mass anisotropy according to, $J_c\ (\theta) = J_c(H_{eff}(\theta))$, where, $H_{eff} = H\varepsilon(\theta)$, and $\varepsilon(\theta) = \left[\sin^2(\theta) + \left(\frac{m_{ab}}{m_c}\right)\cos^2(\theta)\right]^{1/2}$, for θ measured from the tape plane. In this case, the $J_c(\theta)$ curve normally has a minimum when **H** is parallel to the *c*-axis and only one peak at the *a–b* plane due to the mass anisotropy and the intrinsic pinning. For correlated disorder that has a distribution extended in a preferential direction, an additional peak should appear at the angle when the internal field **B** is parallel to the defect. A typical example of correlated defects is the linear amorphous tracks produced by an irradiation with high-energy heavy ions [17,18]. Correlated defects can also be naturally formed during a film synthesis process. For example, the intergrowths formed during the laminar growth in many *ex situ* films are nearly parallel to the *a–b* plane, resulting in a superimposed effect over the intrinsic pinning, raising and broadening the *a–b* peak. On the other hand, a columnar film growth mode may generate correlated defects, such as dislocations, twin and/or grain boundaries, which are nearly parallel to the *c*-axis, yielding an additional J_c peak accordingly [19,20].

From an application standpoint, it is very important to purposely introduce additional defects into the superconducting layer of a coated conductor to enhance the flux pinning. It is expected that additional correlated defects can be tailored to improve the in-field performance not only in the *a–b* plane but also in other directions such that the overall anisotropy in $J_c(\theta)$ is reduced. Among various methods for introducing structural defects, incorporation of non-superconductive nanoparticles has evolved as the most effective one due to its strong effects. *c*-Axis columnar defects (CD's) comprised of nanoparticles of $BaZrO_3$ (BZO) [21–23], $BaSnO_3$ (BSO) [24], or more recently the rare-earth oxides RE_3TaO_7 (RTO) [25] have been introduced into YBCO-based films fabricated by PLD, demonstrating greatly enhanced flux pinning in this direction, analogous to the irradiation-induced defects. BZO nanoparticles have also been proven to be effective in improving flux pinning isotropically when introduced into films made by chemical solution method such as MOD [26]. In-field performance improvement has also been achieved by the formation of a multi-layered structure with nanoparticles of Y_2O_3 [27] or YBa_2CuO_5 (2 1 1) [28] dispersed parallel to the *a–b* plane.

Recently, correlated defects aligned parallel to the *a–b* plane and/or along the *c*-axis have been incorporated into YBCO-based films made by MOCVD [29,30], leading to a significant overall enhancement of the in-field performance. Using IBAD-MgO on Hastelloy as a template, MOCVD has evolved as a successful technology for the practical fabrication of HTS coated conductors because of its capability of producing high quality films with high throughput [31]. In this paper, we have studied the magnetic field angular dependence of J_c of a prototype GdYBCO coated conductor fabricated by the MOCVD technology. BZO as well as $(Y,Gd)_2O_3$ nanoparticles were introduced into the film by doping the precursor with Zr and Gd to the appropriate levels [30]. These nanoparticles are distributed either parallel to the *c*-axis (BZO) or to the *a–b* plane (RE_2O_3) so that flux pinning is enhanced in the respective orientations. Our goal is to establish the relationship between the in-field angular behavior of the coated conductor and its microstructure.

2. Experimental

The GdYBCO film was deposited by MOCVD on an IBAD-MgO template which has a multilayer structure of $LaMnO_3$/homoepitaxial-MgO/IBAD-MgO/Y_2O_3/Al_2O_3/Hastelloy tape. Details about the IBAD-MgO template and the MOCVD process, which uses a liquid precursor delivery system, can be found elsewhere [32]. In previous work [30], it was found that the angular dependence of J_c was impacted mostly by the composition of the films. The composition of the GdYBCO coated conductor studied in this work was $Zr_{0.5}Gd_{0.65}Y_{0.65}Ba_2Cu_3$, where the numbers denote the atomic ratio of the elements in the liquid precursor. With the addition of the extra rare earth elements and Zr, it was shown that arrays of aligned $(Y,Gd)_2O_3$ and BZO nanoparticles formed in the directions parallel to the *a–b* plane and to the *c*-axis, respectively [30]. In addition to composition, deposition temperature and growth rate are among the parameters that influence the in-field performance of

the coated conductor. For the film studied, the deposition temperature was 970 °C and the growth rate was 0.4 μm/min for the superconducting layer. With one pass of deposition, the GdYBCO layer has a thickness of ~0.5 μm, determined by cross-sectional TEM. The as-produced tape was 12 mm in width. A thickness dependence of J_c has been observed for the films made by the MOCVD technology. While the thickness dependence is not a focus of this paper, our property measurements and microstructural characterization were all conducted on samples obtained from the same tape.

The angular dependence of J_c (indeed, the critical current I_c) was measured in a system where sample is cooled by being immersed into liquid nitrogen. Therefore, all the transport data were obtained at ~77 K. In the presence of a horizontally applied magnetic field, the sample is rotated about a vertical axis by a step motor. The sample stage rotation mechanism has an angular resolution of 0.01°. By mounting a sample in different orientations, a J_c could be measured with the electrical current flowing either parallel or perpendicular to the longitudinal axis of the tape. The configuration is shown in Fig. 1, where the current **I** is parallel to the **x**-axis (longitudinal tape axis) in Fig. 1a and to the **y**-axis (transverse tape axis) in Fig. 1b, respectively. In both cases, the direction of the electrical current was kept perpendicular to the applied magnetic field (**I**⊥**H**) for the maximum Lorentz force configuration. Using the conventional four-probe method, all J_c values were determined based on a criterion of 1 μV/cm. The transition temperature was measured resistively in a separate cryostat, yielding the value of T_c = 90.3 K.

The microstructure of the GdYBCO coated conductor was investigated with focus on: (1) the crystalline orientation of the GdYBCO lattice with respect to the film surface; (2) the crystalline orientation relationship between the $(Y,Gd)_2O_3$ and BZO nanoparticles and the GdYBCO lattice; and (3) the spatial orientation of the extended $(Y,Gd)_2O_3$ and BZO nanoparticles. X-ray diffraction was carried out on a Rigaku RU300 diffractometer equipped with a four-circle goniometer. In order to position the film surface, the reflection of a laser beam was used for the collimation with the sample spun around the ϕ-axis of the goniometer. The rocking curves and the pole figures were taken for the relevant phases. The TEM study was carried out using a Philips CM200 FEG TEM microscope. TEM specimens of two different orientations were prepared by focused ion beam (FIB), one with a cross-section within the **y–n** plane and the other with a cross-section within the **x–n** plane of Fig. 1. The microstructures viewed from the two different directions were compared.

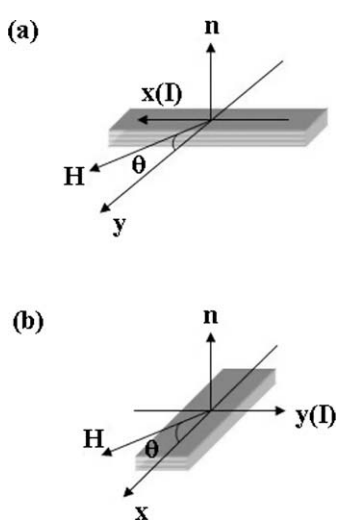

Fig. 1. The configuration for the electrical current (**I**) and the applied magnetic field (**H**) with respect to the tape axis. In (a) **I** is parallel to the longitudinal axis of the tape (**I**||**x**), and in (b) **I** is perpendicular to the tape axis (**I**||**y**). Here, **n** is the normal to the tape surface.

3. Results

The anisotropy of J_c in coated conductors is an important issue for potential applications. One concern for devices with variable magnetic field direction is the lowest $J_c(\theta)$, since this value may determine the tape performance. Measurement of a full-range dependence of J_c, while varying the angle θ (as shown in Fig. 1) between the magnetic field and the film surface from 0° to 360°, can clearly show both weak and strong orientations, where the latter may result from angularly selective flux pinning such as that produced by oriented, extended nanostructures.

A full-range angular dependence of J_c measured at 77 K, 1 T is shown in the polar graph in Fig. 2. The solid curve is for the current flowing parallel to the tape axis (**I**||**x**) as in Fig. 1a, while the dashed curve is for the current perpendicular to the tape axis (**I**||**y**), as in Fig 1b. In both cases, the angular dependence of J_c appears to be essentially polar symmetric; that is, within the experimental error the J_c value measured at certain θ is the same as that measured at 180° + θ. Examination of this feature at low fields (⩽0.1 T), however, revealed differences in the J_c values measured at two orientations 180° apart. The low-field phenomenon was carefully investigated by comparing the J_c values measured with the DC current flowing in the opposite directions. By only switching the current polarity, the direction of the Lorentz force is reversed, which is equivalent to a rotation of the sample from θ to 180° + θ. In this way, any possible geometric effect relating to the rotation mechanism is excluded. It was found that at 0.05 T, for example, the difference in the J_c values, when the Lorentz force direction was reversed, could reach up to 7%, dependent on the field orientation. The exact source of this phenomenon is to be studied separately.

The J_c maxima owing to the correlated flux pinning in two different orientations are obvious in both curves in Fig. 2, one corresponding essentially to the *a–b* plane of the GdYBCO lattice and the other to the columnar BZO nanoparticles. For simplicity, the J_c maxima can be denoted as the *a–b* peak and the *c*-peak, respectively. The difference in the angular dependence of J_c between **I**||**x** and **I**||**y** is clearly evident. For **I**||**x**, which is the case in practical applications, the *a–b* peaks are not at the orientations where **H**||surface and the *c*-peaks are not at the orientations where **H**||**n**; i.e., both J_c peaks are shifted from the symmetry directions of the macroscopic sample. The *a–b* peak shift suggests that there

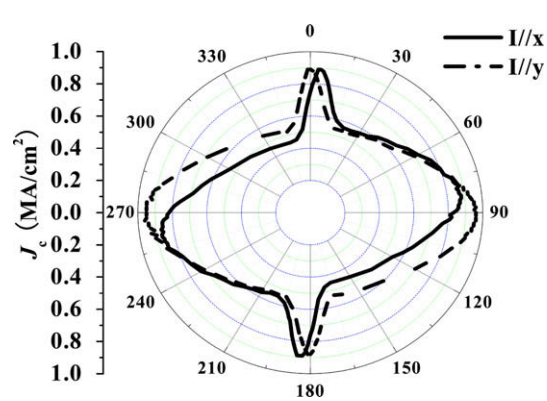

Fig. 2. Magnetic field angular dependence of J_c in a 360° range measured at 77 K and 1 T. The solid curve is for **I**||**x** as in Fig. 1a and the dashed curve is for **I**||**y** as in Fig. 1b. 0° and 180° are where **H**||surface. 90° and 270° are where **H**||**n**.

is a tilt of the *a–b* plane with respect to the tape surface. As the angular spacing between the *ab*- and *c*-peaks is not 90°, it implies that the columns of BZO nanoparticles are not parallel to the *c*-axis of the lattice, i.e., the CD's are also tilted with respect to the lattice. In contrast, for **I**||**y**, no peak shift was observed: the *a–b* peaks and *c*-peaks appeared at **H**||surface and **H**||**n**, respectively. Therefore, the spacing between the *ab*- and *c*-peaks is exactly 90°. This observation is similar to an earlier report by Maiorov et al., where an YBCO film was deposited by PLD on $LaMnO_3$ buffered IBAD-MgO [33]. Comparison of the two $J_c(\theta)$ curves in Fig. 2 suggests that the tilts of the lattice and the CD's only occurred in the **y–n** plane, with no tilt components in the **x–n** plane.

For **I**||**x**, the spacing between the two peaks is not 90° and the minimum J_c in the first and third quadrants (at ~20° and ~200°) is higher than that in the other two quadrants (at ~165° and ~345°). This difference can also be attributed to the tilt of the CD's. In the first and third quadrants, the CD orientations are closer to the *a–b* plane so as to contribute more flux pinning to the minimum J_c, compared with that in the other two quadrants. A relevant consequence is that the *a–b* peak is asymmetric.

These features in $J_c(\theta)$ are directly correlated with the microstructure of the GdYBCO coated conductor, which was characterized using XRD and TEM. Fig. 3 shows the XRD rocking curves taken for the four different phases in the tape. Prior to the ω-scans, the sample orientation was adjusted such that the tape surface normal coincided exactly with the ϕ-axis of the XRD goniometer. The rocking curves shown in the figure are for: (a) LMO (0 0 2), (b) GdYBCO (0 0 5), (c) $(Y,Gd)_2O_3$ (0 0 4), and (d) BZO (0 0 2), respectively, and they were all taken with the diffraction plane parallel to the **y–n** coordinate plane. For each phase, a pair of rocking curves was recorded with the sample rotated about the ϕ-axis by 180°. In this way, the tilt of each phase about the **x**-axis or with respect to the film surface is equal to half of the spacing between the peaks of the two rocking curves. The results showed that the tilts of all the phases were similar and close to 2.3° on average. The out-of-plane textures, $\Delta\omega$, were also determined for the four phases, which were close to 2° (FWHM). On the other hand, when the ω-scans were carried out with the diffraction plane parallel to the **x–n** coordinate plane, the two rocking curves for each phase basically coincided (not shown), indicating that there was no crystalline tilt within the **x–n** plane. In addition, the XRD results showed that the nanoparticles of both $(Y,Gd)_2O_3$ and BZO were coherent with the GdYBCO matrix. Further inspection of the pole figures (not shown) suggested that the nanoparticles were also epitaxial to the matrix in-the-plane with a crystalline relationship of BZO(1 0 0)||$(Y,Gd)_2O_3$(1 1 0)||GdYBCO(1 0 0)||LMO(1 0 0).

The lattice tilt in the GdYBCO film originated from the tilt in the IBAD-MgO that occurred during the IBAD deposition. It was reported that the MgO (100) planes tend to tilt toward the ion source during the IBAD process and the degree of the tilt increases with the MgO layer thickness [34]. The tilt was transmitted epitaxially through the $LaMnO_3$ layer, and subsequently into the superconducting layer during the MOCVD process. For SuperPower's template, the optimal thickness of the IBAD-MgO is 10 nm. At this thickness, the tilt can be as small as a couple of degrees or less, as observed here.

Separate specimens were prepared for TEM study, with cross-sections parallel to the **y–n** plane and parallel to the **x–n** plane, respectively. A quick comparison of the TEM images, shown in Fig. 4a and b, suggested that there are extended tilted structures

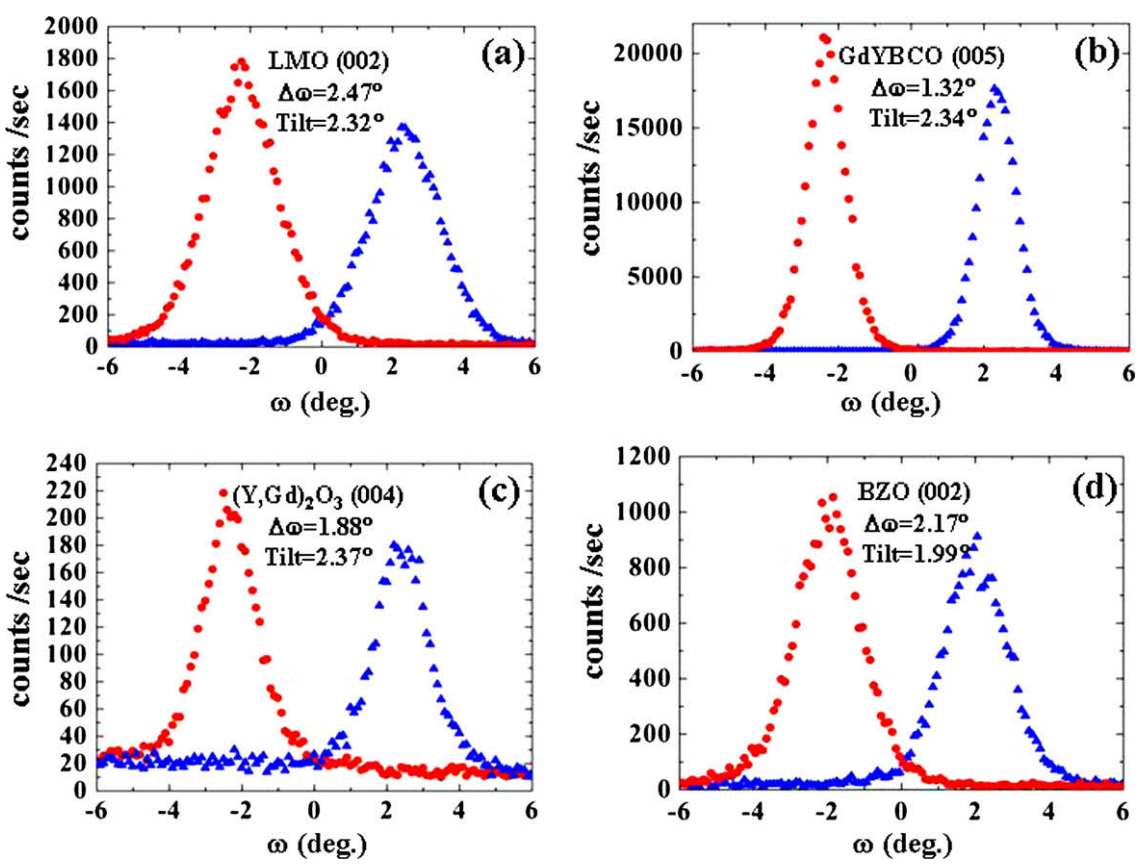

Fig. 3. XRD Rocking curves of: (a) $LaMnO_3$ (0 0 2), (b) GdYBCO (0 0 5), (c) $(Y,Gd)_2O_3$ (0 0 4), and (d) BZO (0 0 2) obtained with ω-scans. Before taking the rocking curves, the orientation of the tape was aligned such that the normal to its surface coincided with the ϕ-axis of the XRD goniometer. For each phase, a pair of rocking curves were taken with the sample rotated about the ϕ-axis by 180°; the diffraction plane was perpendicular to the **x**-axis.

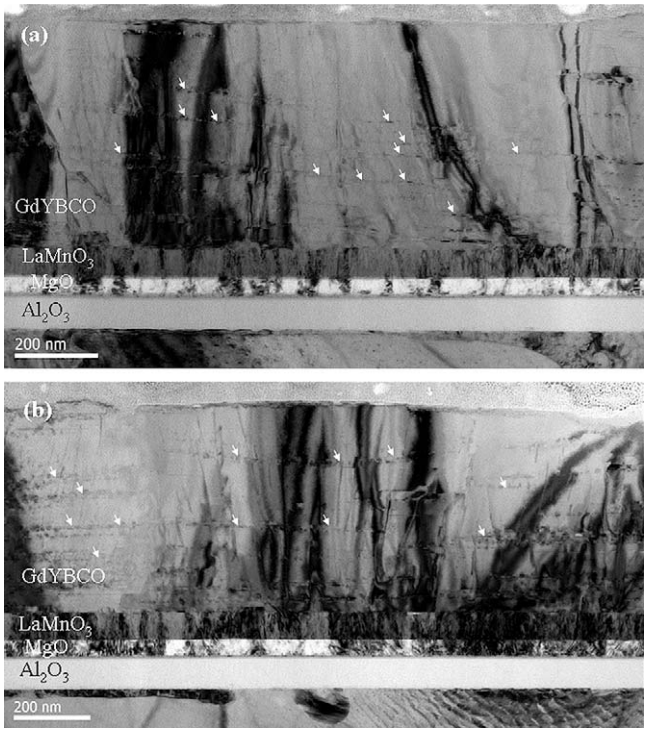

Fig. 4. TEM images for the cross-section within: (a) the **y–n** plane, and (b) the **x–n** plane. A tilt in the structure of about 6–7° in (a) is evident, which is due to the shallow, oblique bias in the stacking of platelet-like extended $(Y,Gd)_2O_3$ nanoparticles. In contrast, no such tilt is seen in (b).

within the **y–n** cross-section, but no tilt within the **x–n** cross-section. Scrutiny at higher magnifications confirmed that the tilt of the GdYBCO lattice with respect to the film surface within the **y–n** cross-section is between 2–3°, but no tilt in the lattice within the other cross-section. This difference is consistent with the XRD findings as well as the $J_c \sim \theta$ relationships given in Fig. 2. The tilt of the extended structure presented in Fig. 4a is actually 6–7°. Further analysis suggested that this tilt is due to a stacking bias of the extended $(Y,Gd)_2O_3$ nanoparticles. A higher magnification TEM image in Fig. 5a reveals that these platelet-like $(Y,Gd)_2O_3$ nanoparticles (indicated by the white arrows) were assembled in an array that tilted relative to the *a–b* plane of the lattice (indicated by the dashed line). As concluded earlier, the $(Y,Gd)_2O_3$ nanoparticles are coherent to the GdYBCO lattice. So, the distribution of these nanoparticles is analogous to a stacking along a staircase. Similar structure was reported by Holesinger et al. [35] in a $(Y,Sm)Ba_2Cu_3O_y$ MOCVD film on an IBAD-MgO template, where the inclined nanoparticles were $(Y,Sm)_2O_3$. While the underlying reason for this relative tilt is unclear at this time, the effect of the sparsely distributed $(Y,Gd)_2O_3$ arrays on $J_c(\theta)$ will be discussed below.

Fig. 5b is a high resolution TEM image taken also from the **y–n** cross-section. It can be seen that the columnar BZO nanoparticles tilt away from the *c*-axis by about 13°, or about 10° from the surface normal. Observation at lower magnification confirmed that this tilt is ubiquitous. Although there is certain dispersion in the angle of the BZO columns, they all tilted toward the opposite side of the surface normal relative to the tilting of the *c*-axis of the lattice. In contrast, a close inspection of the cross-section parallel to the **x–n** plane shows no evidence of tilts of either the GdYBCO lattice or the extended nanoparticles. The mechanism responsible for this phenomenon needs further investigation.

In summary, the microstructural characterizations by XRD and TEM are internally consistent and complementary in their findings. The observed tilts of the *ab*-plane and the extended nanoparticles

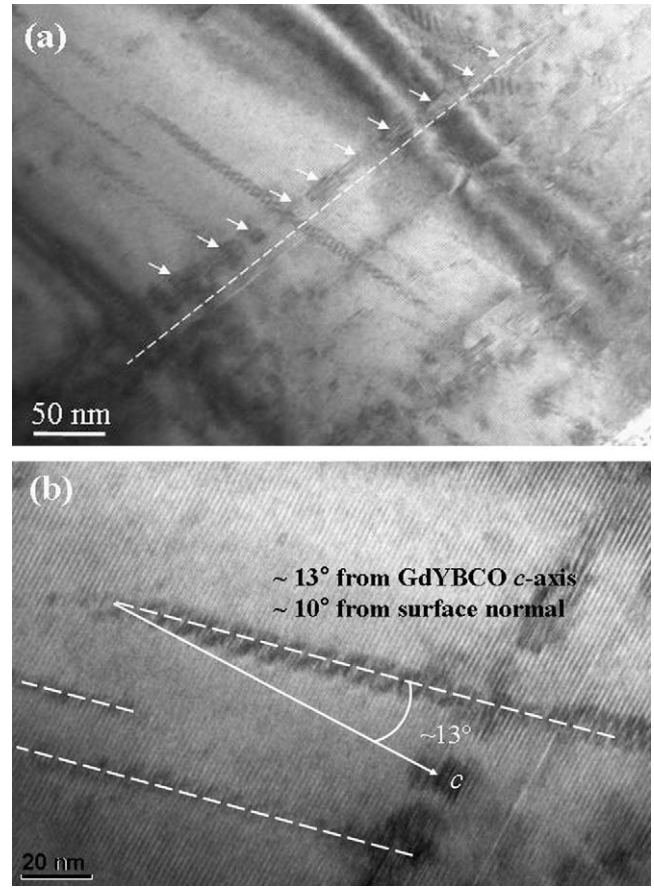

Fig. 5. TEM images for the cross-section within the **y–n** plane: (a) the platelet-like $(Y,Gd)_2O_3$ nanoparticles (indicated by the white arrows) were assembled in an array tilting relatively to the GdYBCO *a–b* plane (indicated by the dashed line) and (b) the columnar BZO nanoparticles are stacked with a tilt about 13° from the *c*-axis of the lattice, or about 10° from the surface normal.

coincide well with the J_c-peak positions in Fig. 2: the *ab*-peaks at 1 T occur at 2–3° and 0° for the respective cases, while the *c*-axis peaks occur near 10° and 0° from the surface normal, respectively. Thus, the multiple anisotropies manifested in Fig. 2 (where the applied field is large enough to ensure that the internal field **B** or the vortices are nearly parallel to **H**) clearly originate from the observed microstructural features.

With this perspective, we next establish the effect of magnetic field strength on the angular dependence of J_c. Since the curves in Fig. 2 are essentially twofold symmetric, further measurements were conducted in a 180° range. Shown in Fig. 6a and b are the J_c versus applied field orientation relationships at 77 K for **I**||**x** and **I**||**y**, respectively, with the magnitude of the field ranging from 0.05 T to 1.5 T. For **I**||**x**, the *a–b* peak was at about 2.8° in the maximum field $H = 1.5$ T. With decreasing H, the *a–b* peak position progressively shifted to larger angles and reached about 6.7° for $H = 0.05$ T. In contrast, there was no observable shift in the *c*-peak positions upon the changing of the field magnitude. Here, a broad J_c peak develops in fields $H \geqslant 0.25$ T with a maximum near 81° (9° from the surface normal, independent of H), where the peak shift from 90° is due to the tilt of the columnar BZO nanoparticles discussed above. The angular spacing between the *ab*- and *c*-peaks is less than 90°, i.e., 74–78°, indicating that the curves were obtained in the first or the third quadrant as seen in Fig. 2. In the case with **I**||**y**, there was no shift in the peak positions with the varying field intensity for either the *ab*- or the *c*-peak, as shown in Fig. 6b. This again confirms the symmetric nature of the structure projected in the **x–n** plane.

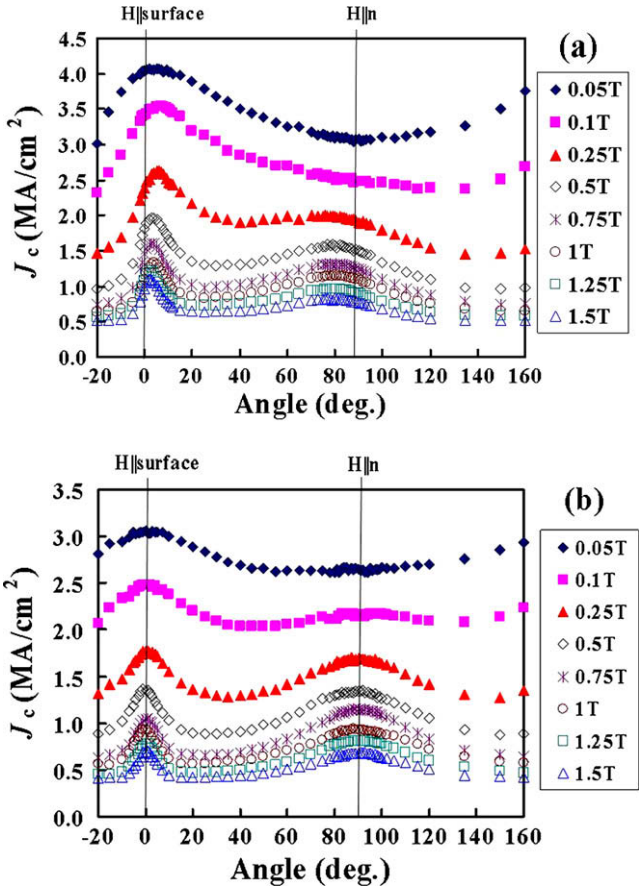

Fig. 6. Magnetic field angular dependence of J_c at 77 K in a 180° range with H ranging from 0.05 T to 1.5 T. (a) When **I**||**x** as in Fig. 1a and b when **I**||**y** as in Fig. 1b. Angles are defined such that 0° is where **H**||surface and 90° is where **H**||**n**. For the case of (a) when the current is parallel to the tape axis, a field-magnitude-dependent shift of the *ab*-peak position can be seen.

As briefly discussed above, the relative orientation of **B** with respect to **H** is determined by several factors, including the magnitude of **H**, the geometry effect, the anisotropy of the superconducting material and possible strong pinning from correlated defects. In addition, there may be self field effects arising from the transport currents. The misalignment between **B** and **H**, which could be significant at low field, is visible when there is certain asymmetry in the structure such as tilted lattice and/or tilted correlated defects that act as effective pinning source. The indicator is that the peak(s) within the $J_c \sim \theta$ relationship may shift upon the change of the field strength. It has been shown that highly parallel tilted structures can act passively as detectors for the orientation of the internal field **B** [36]. In that previous work, Silhanek et al. analyzed the free energy according to the competition between the geometry effect (tending to make **B** perpendicular to the plane of plate-like crystals) and the crystalline anisotropy (tending to make **B** parallel to the plane, to minimize the vortex energy per unit length). Minimization of the free energy led to an expression where the misalignment between **B** and **H** is proportional to $1/H$. In that case, for YBCO single crystals with parallel off-*c*-axis CD's introduced by heavy ion irradiation, shifts in the peak position of the irreversible magnetization ($\sim J_c$) were observed as the magnitude of the applied field was varied. Their experimental findings, including the sign of the shift and its field and temperature dependence, were quite consistent overall with the free energy analysis.

In contrast to those findings, in the present work the tilted BZO columnar nanoparticles in the GdYBCO coated conductor produce no observable shift in the peak positions as in Fig. 6a. We note that these peaks are broad, due in part to angular spread (splay) in the BZO columns. Indeed, the baseline $J_c(\theta)$ evolves with field, which may itself be reflective of changes in **B** versus **H** direction, and the peak even disappears below about 0.25 T. With all the competing effects in the superconductor and the complex microstructural features, it is perhaps not surprising that finer details be washed out.

The shift in the *a–b* peak position with respect to field magnitude, shown in Fig. 6a, is qualitatively inconsistent with the free energy arguments above, with the *sign* or sense of the peak shift to be opposite to that expected from the expressions of Silhanek et al. [36]. A similar sign reversal was found in a previous study of the effect of the lattice tilt on the *a–b* peak position by Maiorov et al. [33]. Compared with the material of Maiorov et al., the present coated conductor is more complicated, since there is not only a tilt of the GdYBCO lattice but also a tilt of the extended nanoparticles of $(Y,Gd)_2O_3$ that act as flux pinning source. However, the present observations are in agreement with those of Holesinger et al. [35], implying the effect of strong low-field pinning by the slightly tilted $(Y,Gd)_2O_3$ precipitate stacks shown in the TEM micrograph of Figs 4a and 5a. These tilted, well-aligned arrays are much extended but sparsely distributed. They could accommodate matched vortex strong trapping only at low flux densities. Indeed, high resolution TEM shows the presence of many more, but shorter, *a–b* oriented nanoparticles that could provide dominant pinning at progressively higher fields, see Fig. 7. Then, the evolution with field strength of the *a–b* peak from an angular position of ~6.7° toward alignment with the lattice planes at ~2.8° may be due to a progression of vortex matching to the operative pinning nanostructure. While the sign of the peak position shift was opposite to what predicted by the equilibrium energetics analysis, it is interesting that the *a–b* peak position was still observed to shift roughly in accord with $1/H$, as shown in Fig. 8, where an extrapolation to infinite field gives a peak position closely coincident with the observed tilt of the *a–b* planes. The exact mechanism underlying the observed

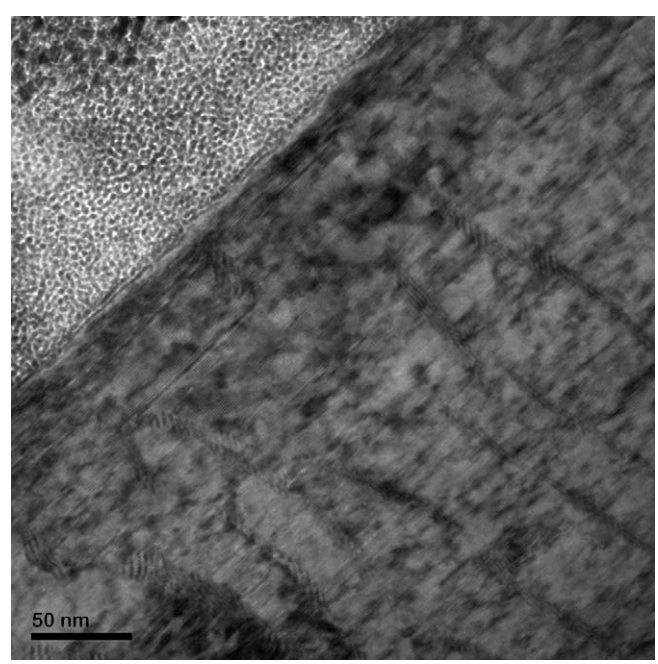

Fig. 7. TEM images for the cross-section within the **y–n** plane. In addition to the BZO nanoparticle columns, there are many platelet-like $(Y,Gd)_2O_3$ nanoparticles oriented nearly parallel to the *a–b* plane. They do not form long arrays, but may contribute significantly to the flux pinning at higher fields due to their denser distribution.

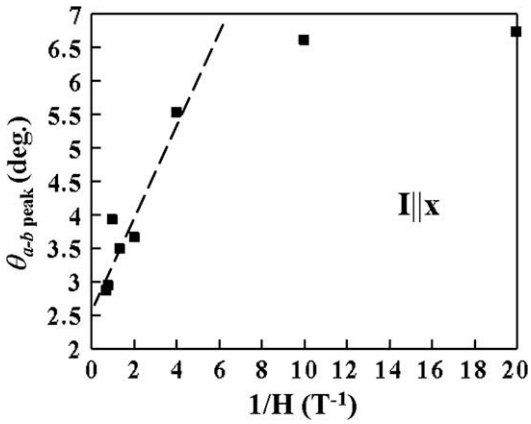

Fig. 8. Angular position of the *ab*-peak, as shown in Fig. 6a, versus reciprocal of the applied field magnitude for current flowing along the tape axis (**I**||**x**).

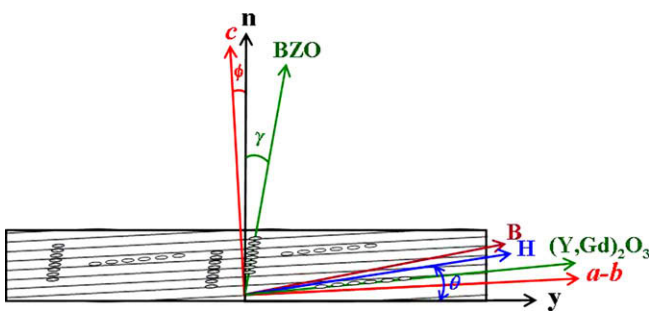

Fig. 9. Configuration schematic within the **y–n** plane as viewed along the longitudinal axis of the tape. The expected misalignment between **B** and **H** is indicated. Here, θ is the angle between **H** and **y**. ϕ is the tilt of the lattice *c*-axis with respect to the surface normal **n**. γ is the tilt of the BZO nanoparticle columns from **n**. The tilt of the obliquely stacked $(Y,Gd)_2O_3$ nanoparticle array (6–7°) is larger than the tilt of the *a*–*b* plane (2–3°), with respect to the film/substrate interface. For clarity, the schematic is not drawn in scale.

$1/H$ dependence is unknown. Moreover, it is possible that other contributions to the vortex state energy from self field effects and additional disorder may be significant, especially in low applied fields.

As a schematic summary of the observations, Fig. 9 sketches the characterized microstructural features and the expected misalignment between internal field **B** and external field **H**, corresponding to the case when **I**||**x**. If there are no operative tilts in the structure, e.g., as in the case when **I**||**y**, no J_c peak shift can be observed.

4. Conclusion

We have studied the magnetic field orientation dependence of the critical current density (J_c) of a prototype GdYBCO coated conductor fabricated by MOCVD on IBAD-MgO. With the angle between the magnetic field and the tape surface varying from 0° to 360°, the angular dependence of J_c is essentially twofold symmetric. Peaks in $J_c(\theta)$ were found to be correlated with extended flux pinning nanostructures oriented nearly parallel to the superconductor's *a*–*b* plane and the crystalline *c*-axis. Transport measurements were conducted with the current flowing along or perpendicular to the longitudinal axis of the conductor tape. Profiles of $J_c(\theta)$ at the orthogonal currents were compared, demonstrating the symmetry and asymmetry in flux pinning. When the current was flowing along the tape axis, asymmetries in the angular positions of the maximum flux pinning effects, along with the field-strength dependent shift of the *ab*-peak position, were observed. With the current flowing perpendicular to the tape axis, the *ab*-peak and *c*-peak showed no shifts and were positioned with the magnetic field parallel and perpendicular to the film surface, respectively.

Details of the angularly dependent J_c were related to the microstructure of the coated conductor, characterized using XRD and TEM. It was found that the GdYBCO lattice is tilted by 2–3° transverse to the tape axis, and both $BaZrO_3$ and $(Y,Gd)_2O_3$ nanoparticles were epitaxial to the GdYBCO matrix. TEM studies indicated that columnar stacks of BZO nanoparticles tilt about 13° from the GdYBCO *c*-axis in the plane perpendicular to the tape axis. The BZO columns, with some angular spread, are tilted away from the surface normal, opposite to the tilting of the GdYBCO *c*-axis. The platelet-like $(Y,Gd)_2O_3$ nanoparticles have two different distributions. Some of them form extended, well-aligned oblique arrays that are sparsely distributed. The tilt of these stacking arrays is about 6–7° from the tape surface, or about 4° relative to the *a*–*b* plane. Other $(Y,Gd)_2O_3$ nanoparticles have nearly random distribution, but with their longer laterals roughly parallel to the *a*–*b* plane, contributing to the flux pinning along this direction. The unique nanostructures of the GdYBCO coated conductor, with or without the tilts of both the lattice and the extended nanoparticles, account for the observed asymmetry and symmetry in the flux pinning, and are responsible for the rich angular dependence of J_c.

It is worth to emphasize that all the observed tilts are exclusively in the direction transverse to the tape axis, suggesting that the tilt of the IBAD-MgO could be the sole source. With the establishment of the relationship between $J_c(\theta)$ and the microstructure, further investigation is required to understand the mechanism that produces the unique structure. Why do the BZO columns and the GdYBCO tilt in the opposite directions? What causes the $(Y,Gd)_2O_3$ nanoparticles to have different distributions? Answers to the questions like these would be helpful in tuning and optimizing the microstructure so as to further enhance the flux pinning and reduce the J_c anisotropy. Interesting follow-up work includes, for example, studying BZO-doped multi-pass thicker films and exploring possible effects of post-deposition treatments. The effects of the misalignment between internal field **B** and external field **H** on J_c anisotropy in a complex system like this also needs to be further investigated.

Acknowledgements

Research sponsored by the US Department of Energy – Office of Electricity Delivery and Energy Reliability, Superconductivity Program for Electric Power Systems under contract DE-AC05-00OR22725 with Oak Ridge National Laboratory, managed and operated by UT-Battelle, LLC.

References

[1] S.R. Foltyn, L. Civale, J.L. MacManus-Driscoll, Q.X. Jia, B. Maiorov, H. Wang, M. Maley, Nat. Mater. 6 (2007) 631.
[2] a M. Tachiki, S. Takahashi, Solid State Commun. 70 (1989) 291;
b M. Tachiki, S. Takahashi, Solid State Commun. 72 (1989) 1083.
[3] B. Roas, L. Schultz, G. Saemann-Ischenko, Phys. Rev. Lett 64 (1990) 479.
[4] L. Civale, B. Maiorov, J.L. MacManus-Driscoll, H. Wang, T.G. Holesinger, S.R. Foltyn, A. Serquis, P.N. Arendt, IEEE Trans. Appl. Supercond. 15 (2005) 2808.
[5] J.Y. Coulter, J.O. Willlis, M.M. Mann, P.C. Dowden, S.R. Foltyn, P.N. Arendt, J.R. Groves, R.F. DePaula, M.P. Maley, D.E. Peterson, IEEE Trans. Appl. Supercond. 9 (1999) 1487.
[6] T. Horide, K. Matsumoto, Y. Yoshida, M. Mukaida, A. Ichinose, S. Horii, K. Osamura, Jpn J. Appl. Phys. 44 (2005) L111.
[7] H. Zhang, H. Wu, C. Ren, G. Chen, Supercond. Sci. Technol. 7 (1994) 359.
[8] C. Dubourdieu, O. Lebedev, G. Delabouglise, F. Weiss, U. Schmatz, J.P. Senateur, J. Alloys Compd. 251 (1997) 351.
[9] L. Civale, B. Maiorov, A. Serquis, S.R. Foltyn, Q.X. Jia, P.N. Arendt, H. Wang, J.O. Willis, J.Y. Coulter, T.G. Holesinger, J.L. MacManus-Driscoll, M.W. Rupich, W. Zhang, X. Li, Physica C 412–414 (2004) 976.

[10] E.F. Talantsev, N.M. Strickland, P. Hoefakker, J.A. Xia, N.J. Long, Curr. Appl. Phys. 8 (2008) 88.
[11] D.H. Lowndes, D.K. Christen, C.E. Klabunde, Z.L. Wang, D.M. Kroeger, J.D. Budai, S. Zhu, D.P. Norton, Phys. Rev. Lett. 74 (1995) 2355.
[12] J.D. Budai, W. Yang, N. Tamura, J. Chung, J.Z. Tischler, B.C. Larson, G.E. Ice, C. Park, D.P. Norton, Nat. Mater. 2 (2003) 487.
[13] P.S. Czerwinka, R.P. Campion, K.F. Horbelt, P.J. King, S. Misat, S.M. Morley, H.U. Habermeier, B. Leibold, Physica C 324 (1999) 96.
[14] J.R. Groves, P.N. Arendt, S.R. Foltyn, Q. Jia, T.G. Holesinger, L.A. Emmert, R.F. DePaula, P.C. Dowden, L. Stan, IEEE Trans. Appl. Supercon. 13 (2003) 2651.
[15] Y. Sato, S. Honjo, Y. Takahashi, K. Muranaka, K. Fujino, T. Taneda, K. Ohmatsu, H. Takei, Physica C 378–381 (2002) 1118.
[16] M. Bauer, R. Metzger, R. Semerad, P. Berberich, H. Kinder, Mat. Res. Soc. Symp. Proc. 585 (2000) 35.
[17] B. Holzapfel, M. Leghissa, P. Bauer, G. Kreiselmeyer, M. Kraus, S. Bouffard, L. Schultz, G. Saemann-Ischenko, J. Supercond. 7 (1994) 205.
[18] A.V. Silhanek, L. Civale, J. Low Temp. Phys. 135 (2004) 157.
[19] K. Develos-Bagarinao, H. Yamasaki, M. Murugesan, Y. Mawatari, Y. Nakagawa, J.C. Nie, Supercond. Sci. Technol. 18 (2005) S266.
[20] A. Diaz, L. Mechin, P. Berghuis, J.E. Evetts, Phys. Rev. Lett. 80 (1998) 3855.
[21] J.L. Macmanus-Driscoll, S.R. Foltyn, Q.X. Jia, H. Wang, A. Serquis, L. Civale, B. Maiorov, M.E. Hawley, M.P. Maley, D.E. Peterson, Nat. Mater 3 (2004) 439.
[22] A. Goyal, S. Kang, K.J. Leonard, P.M. Martin, A.A. Gapud, M. Marela, M. Paranthaman, A.O. Ijaduola, E.D. Specht, J.R. Thompson, D.K. Christen, S.J. Pennycook, F.A. List, Supercond. Sci. Technol. 18 (2005) 1533.
[23] Y. Yamada, K. Takahashi, H. Kobayashi, M. Konishi, T. Watanabe, A. Ibi, T. Muroga, S. Miyata, Appl. Phys. Lett. 87 (2005) 132502.
[24] C.V. Varanasi, J. Burke, L. Brunke, H. Wang, M. Sumption, P.N. Barnes, J. Appl. Phys. 102 (2007) 063909.
[25] S.A. Harrington, J.H. Durrel, B. Maiorov, H. Wang, S.C. Wimbush, A. Kursumovic, J.H. Lee, J.L. MacManus-Driscoll, Supercond. Sci. Technol. 22 (2009) 022001.
[26] J. Gutierrez, A. Llordes, J. Gazquez, M. Gibert, N. Roma, S. Ricart, A. Pomar, F. Sandiumenge, N. Mestres, T. Puig, X. Obradors, Nat. Mater. 6 (2007) 367.
[27] A.A. Gapud, D. Kumar, S.K. Viswanathan, C. Cantioni, M. Varela, J. Abiade, S.J. Pennycook, D.K. Christen, Supercond. Sci. Technol. 18 (2005) 1502.
[28] T. Haugan, P.N. Barnes, R. Wheeler, F. Meisenkothen, M. Sumption, Nature 430 (2004) 867.
[29] L. Stan, T.G. Holesinger, B. Maiorov, Y. Chen, D.M. Feldmann, I.O. Usov, R.F. DePaula, V. Selvamanickam, L. Civale, S.R. Foltyn, Q.X. Jia, Supercond. Sci. Technol. 21 (2008) 105023.
[30] Y. Chen, V. Selvamanickam, Y. Zhang, Y. Zuev, C. Cantoni, E. Specht, M.P. Paranthaman, T. Aytug, A. Goyal, D. Lee, Appl. Phys. Lett. 94 (2009) 062513.
[31] V. Selvamanickam, Y. Chen, X. Xiong, Y.Y. Xie, M. Martchevski, A. Rar, Y. Qiao, R.M. Schmidt, A. Knoll, K.P. Lenseth, C.S. Weber, IEEE Trans. Appl. Supercond. 19 (2009) 3225.
[32] Y. Chen, X. Xing, Y. Xie, Y. Qiao, X. Zhang, A. Rar, M. Martchevskii, R. Schmidt, K. Lenseth, D. Hazelton, V. Selvamanickam, Mat. Res. Soc. Symp. Proc. 1099 (2008). 1099-II01-2.
[33] B. Maiorov, B.J. Gibbons, S. Kreiskott, V. Matias, T.G. Holesinger, L. Civale, Appl. Phys. Lett. 86 (2005) 132504.
[34] J.R. Groves, P.N. Arendt, S.R. Foltyn, Q. Jia, R.F. DePaula, P.C. Dowden, J. Kung, T.G. Holesinger, L. Stan, L.A. Emmert, E.J. Peterson, Mat. Res. Soc. Symp. Proc. 666 (2001) F10.
[35] T.G. Holesinger, B. Maiorov, O. Ugurlu, L. Civale, Y. Chen, X. Xiong, Y. Xie, V. Selvamanickam, Supercond. Sci. Technol. 22 (2009) 045025.
[36] A.V. Silhanek, L. Civale, M.A. Avila, Phys. Rev. B 65 (2002) 174525.